Mathematical Modelling of Collagen Fibers Rearrangement During Tendon Healing Process

José A. Carrillo, Martin Parisot, Zuzanna Szymańska

Mathematical Modelling of Collagen Fibers Rearrangement During Tendon Healing Process

José Antonio Carrillo
Mathematical Institute, University of Oxford,
Oxford OX2 6GG, United Kingdom
carrillo@maths.ox.ac.uk

Martin Parisot
Inria-Bordeaux, Team CARDAMOM, Office B426,
200 av. de la vieille tour, 33405 Talence Cedex, Bordeaux, France
martin.parisot@inria.fr

Zuzanna Szymańska
Institute of Mathematics, Polish Academy of Sciences
ul. Śniadeckich 8, 00-656 Warsaw, Poland
ICM, University of Warsaw,
ul. Tyniecka 15/17, 02-630 Warsaw, Poland
zszymanska@impan.pl, z.szymanska@icm.edu.pl

April 8, 2020

Abstract

Tendon injuries present a significant clinical challenge to modern medicine as they heal slowly and rarely recover the structure and mechanical strength of a healthy tendon. Moreover, tendon represents a highly under-researched tissue with the process of healing not fully elucidated. To improve the understanding of tendon function and healing process we propose a new model of collagen fibers rearrangement during tendon

healing. The model consists of integro-differential equation describing the dynamics of collagen fibers distribution. We further reduce the model in a suitable asymptotic regime leading to a nonlinear non-local Fokker-Planck type equation for the spatial and orientation distribution of collagen fiber bundles. The reduced model allows for possible parameter estimation based on data due to its simplicity. We showcase some of the qualitative properties of this model simulating its long time asymptotic behavior and the total time for tendon fibers to align in terms of the model parameters. A possible biological interpretation of the numerical experiments performed leads us to the working hypothesis of the importance of the tendon cell size in patients' recovery.

***Keywords*—** Collagen remodelling, Mathematical model, Tendon healing, Integro-differential equations, Alignment

1 Introduction

Tendon injuries, although not directly threatening the lives of affected persons can significantly lower their quality of life [39]. Despite the enormous progress of medicine over the last decades little has been achieved in improving the treatment of these injuries. A significant obstacle in the research is the difficulty with setting up a proper experimental environment, as it is generally not possible to biopsy healthy tendon tissues from patients or volunteers [40]. At present most of the injuries are treated by surgical repair and/or conservative approaches such as physical rehabilitation and cryotherapy [47]. The healing tissue tends to form fibrovascular scars and possesses inferior mechanical and biochemical properties as compared to intact one [47]. Only recently, with the development of regenerative medicine, new treatment perspectives have emerged. However, their effective implementation requires a thorough understanding of the healing process, which due to specific tendon morphology, low cellularity, and poor blood supply, is particularly difficult and where mathematical modeling may provide additional insight [38].

Until now the modeling of the process of tendon healing has virtually not been addressed in the literature. Moreover, despite sharing a lot of similarities with other types of wound healing, the process is beyond the range of applicability of the classical wound healing models. The reason is that classical wound healing models do not focus on collagen fibers structure, which in most tissues does not play such a role as in a tendon. In the case of tendon healing, an adequate description of the reconstruction of the parallel structure of collagen fibers is absolutely essential. Therefore, what may appear surprising at first glance, a mathematical description of tendon healing may draw more from models of the alignment processes of individuals such as fish shoals

or flocks of birds [21, 14, 7, 22, 1, 6, 36, 28]. Although the nature of the described phenomena is different, collagen fibers tend to align in a similar way as individuals in the other models of alignment.

Only recently a simple model of collagen remodeling occurring in the latter stage of the tendon healing process was proposed by Dudziuk at al. [20]. The authors propose an integro-differential equation describing the dynamics of the probability density of collagen fibers in space and orientation. They also show that depending on initial data solutions may either exist globally in time or blow-up in L^∞, i.e. concentration in orientation, in a finite time. The latter behavior can be interpreted as injury healing without scar formation. In the present paper, we build on this statistical description based on fiber bundles orientation by including novel local alignment interactions between the fiber bundles in the model.

Finally, we would like to raise one more issue namely, most of the biophysical models miss a genuine connection to experimental data, which results in the limited predictive value of these models. Usually, it is due to the difficulty in reliable measurement of parameters. However, this difficulty might be overcome by applying an inverse problem approach, that, despite being a considerable challenge, has already been successfully implemented for some biological models, like size-structured models of cell division with non-local kernels [37, 19, 17, 18, 16]. However, one has to bear in mind, that such parameter estimation is commonly very costly in terms of computational resources. Notably, if the number of parameters is large. This refers also to the alignment kernels that usually contain many parameters. Therefore, we consider the reduction of the model, which decreases the number of parameters possibly facilitating the parameter estimation, as one of our main achievements within our work.

This paper is structured as follows. First, in Section 2 we discuss the main biological aspects of tendon tissue and healing process after an injury. In Section 3 we introduce the mathematical model and its associated reduction via an asymptotic limit. Section 4 is devoted to the description of the numerical method used to simulate the reduced model and to present the results of simulations. Moreover, we explore the qualitative properties of the reduced mathematical model, also discussing the impact of particular parameters on total healing time. In Section 5 we finish by giving conclusions and direction of future research.

2 Biology of the tendon

Tendon structure

Tendons are regular bands of fibrous connective tissue that connect muscles to bones and enable transmission of forces, thereby ensuring joint movements [46, 48]. They are

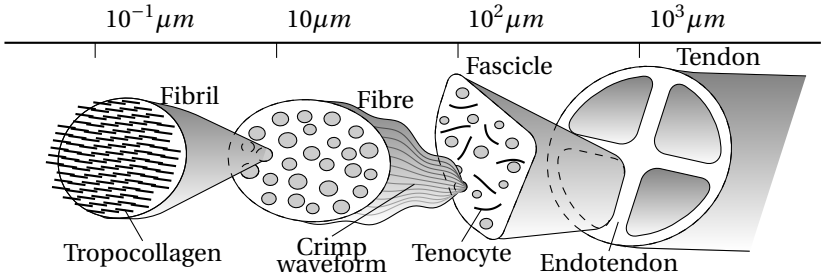

Figure 1: Collagen within tendon has hierarchical structure of increasing complexity: fibrils, fibers (primary bundles), fascicles (secondary bundles), tertiary bundles and tendon itself [25, 38].

build of i) collagen and elastin fibers tightly arranged in parallel; ii) relatively low number of residing tendon cells; iii) and special, strongly hydrophilic ground substance surrounding cells and fibers which enable the rapid diffusion of water-soluble molecules and cell migration [33, 38]. Collagen and elastin fibers account for 70% and 2% of the dry weight of a tendon, respectively [26]. The type I collagen forms 95% of all tendon collagen and consists of clearly defined, parallel, and wavy bundles essentially aligned longitudinally [29, 33]. Collagen fibers are made from fibrous protein subunits linked together to form a long and straight fibers [48]. Aligning the collagen fibers along the long axis of the tendon results in a highly anisotropic tissue, particularly well suited to withstand high uniaxial tensile forces [27, 42]. A healthy tendon is also built to a small extent from elastin and type III collagen [26, 27, 33]. In contrast to type I, the type III collagen does not have such a regular, parallel structure and its fibers can be described as rather disorganized.

Tendon tissue is characterized by low cellularity and poor blood supply [12]. About 90% to 95% of the cellular elements of the tendon are tendon-specific fibroblasts, i.e. tenocytes and its immature form tenoblasts [26, 33]. Tenocytes are spindle-shaped longitudinal cells that lies sparingly in rows between collagen fibrils, whereas more rounded tenoblasts are motile and highly proliferative [33, 38]. Tenocytes and tenoblasts are known to be responsible for producing subunits of collagen fibers, degrading enzymes, and cytokines to maintain the dynamic equilibrium of both the fibrous and non-fibrous components of the tendon [41].

The physiological properties of the tendon are mainly due to its hierarchical structure of increasing collagen complexity: fibrils, fibers (primary bundles), fascicles (secondary bundles), tertiary bundles and the tendon itself [38]. Tenocytes lies sparingly in rows between the bundles of type I collagen fibers [33]. Figure 1 presents the structure of the tendon.

Tendon healing process

The tendon healing process that follows acute injures proceeds in stages similar to those taking place in the healing of other connective tissue injuries. It can be divided into three consecutive but overlapping phases: i) inflammatory; ii) proliferative; and iii) remodelling one [38, 47]. Poor blood supply and low cellularity makes the healing process much more difficult and long-lasting [2].

The **inflammatory phase** starts immediately after the injury. At the place of blood vessels rupture the blood clot begins to form. The blood clot activates the tissue-resident mast cells settled in vicinity of blood vessels to release the inflammatory signals. Inflammatory signals attract and activate inflammatory cells such as neutrophils, monocytes, and macrophages that migrate from surrounding tissue towards the site of injury [30]. The inflammatory cells phagocyte the necrotic tissue, break down the clot initiate the recruitment and activation of tendon specific fibroblasts, i.e. tenocytes and tenoblasts [3, 30, 47].

The **proliferative stage** begins a few days after the injury [47]. Tendon fibroblasts migrate and proliferate about the injury site where they synthesize components of extracellular matrix - most of all new collagen which for the time being is a mainly disorganized type III collagen [3, 15, 38, 47]. At the same time, neutrophils level start to decline whereas macrophages continue to release growth factors that activate and direct cells recruitment towards injury site [47]. Several cytokines are released to promote fibroblast or endothelial proliferation, synthesis of extracellular matrix proteins, cell migration, and differentiation [31]. Synthesis of type III collagen peaks during this stage [38]. Water content remains high during this phase [38].

The **remodeling phase** begins roughly 8 weeks after the injury and consists of resizing and reshaping of the healing tissue [38]. It is further divided into consolidation and maturation stages [15, 38]. During the consolidation stage the tissue changes from cellular to fibrous. Tenocyte metabolism remains high, and collagen fibers become aligned in the direction of stress [47]. The ratio of type I to type III collagen changes in preference to type I during this time [32]. During the maturation stage collagen growth slows down, tenocyte metabolism and tendon vascularity decline [38].

In clinical practice tendon healing if at all is usually monitored by relatively harmless to the patient means of medical imaging methods such as MRI protocols or ultrasound examinations. Although, these methods do not give the full picture as collagen fibers can not be visualized directly they provide important information on changes in volume and edema as well as the internal structure of the tendon. The healthy tendon appears on MRI images as black and internally uniform with no apparent differences. This is mainly related to the proper structure of collagen fibers and very low cellular, water and fat content, i.e. very low amount of hydrogen nuclei that are visible in MRI. The damaged tendon appears much clearer, mostly in gray shades, and internally in-

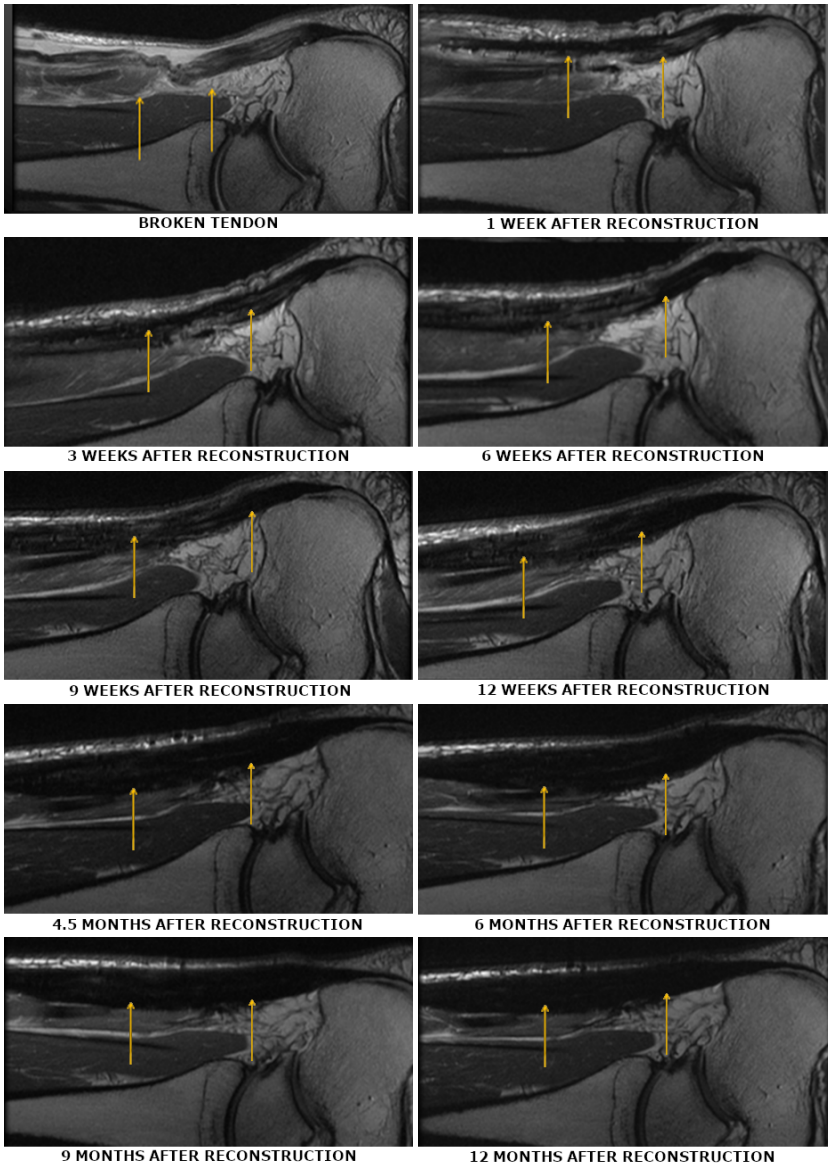

Figure 2: Sequence of sagittal sections of a ruptured tendon taken before the reconstruction and within first year after the reconstructive surgery. Yellow arrows indicate the tendon.

homogeneous. This is mainly because of inflammation, edema and presence of cells

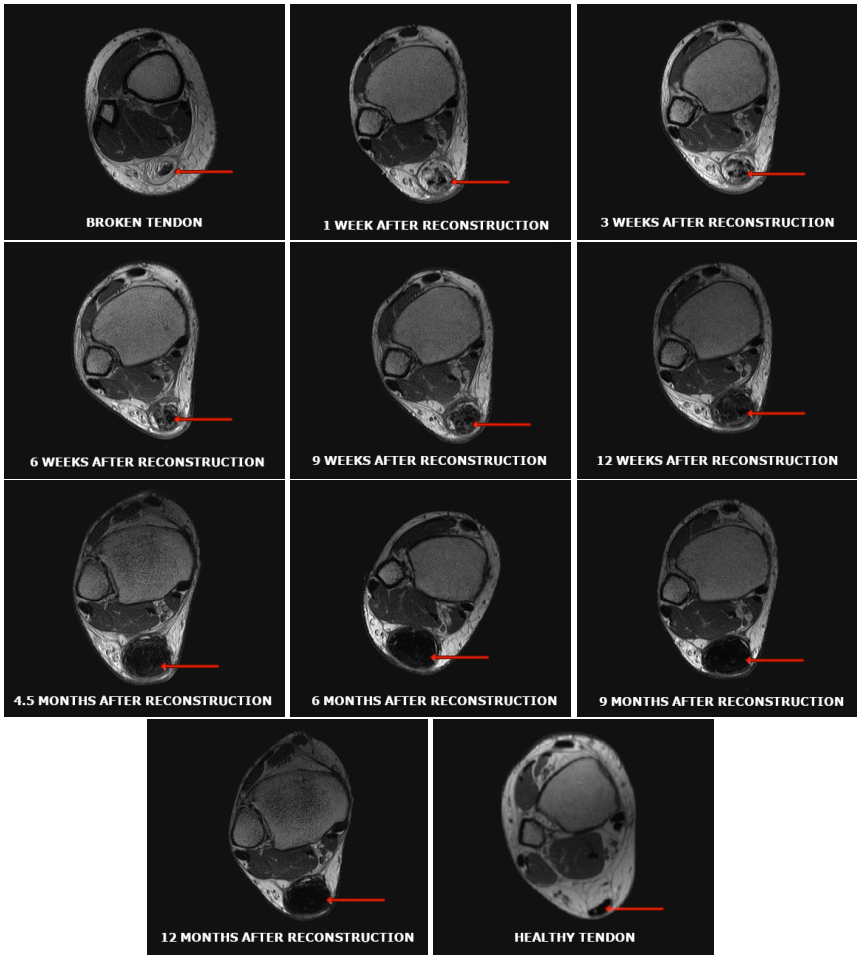

Figure 3: Sequence of cross-sections of a ruptured tendon taken before the reconstruction and within first year after the reconstructive surgery. For comparison, the last image shows the cross-section of a healthy tendon. Red arrows indicate the tendon.

responsible for the healing process.

Figures 2 and 3 present sequences of MRI images monitoring tendon healing process following surgical reconstruction. Within the first weeks, the changes in the MRI are very clear. From about the sixth month or slightly earlier, during the consolidation stage, the changes in the MRI become poorly noticeable. At this time collagen conversion occurs rather than collagen growth. The model we propose approximates exactly

this stage of tendon healing.

3 Mathematical model

Considering its hierarchical structure we model the tendon as a large collection of fiber bundles. For the sake of clarity, our mathematical description corresponds to the level of the fascicle composed of fiber bundles and rows of tenocytes, cf. Figure 1. The mutual influence of fibers that within the living tissue is mediated by tenocytes, in the model is captured by non-local terms, ipso facto we omit an explicit description of the tenocytes. Moreover, we assume that the fiber bundles are already stretched which allows us to treat them as hard sticks without any elastic property. Summarising, we approximate the tendon tissue by a collection of interacting hard sticks characterized by their orientation, that we denote by ϕ. More precisely, ϕ stands for the acute angle between the tangent of the fiber and the axis of a healthy tendon, see Figure 4.

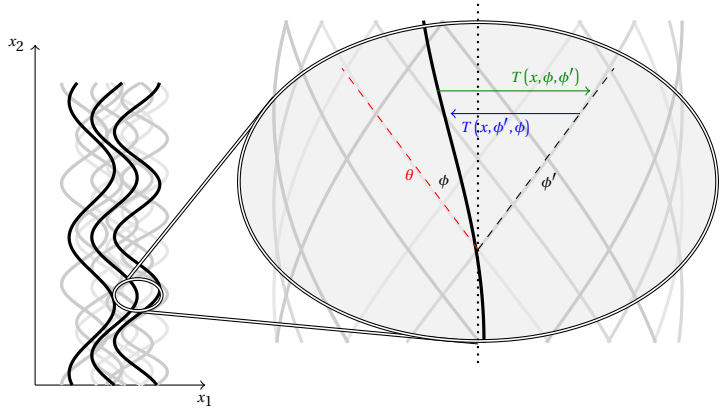

Figure 4: Illustration of the connection between mathematical and biological objects. The left side of the image shows a bundle of interacting collagen fibers, whereas the right side shows its magnification at point x. Turning rate $T(x,\phi',\phi)$ (blue arrow) models the probability that collagen fiber with orientation ϕ' (black dashed line) rearranges into a fiber with orientation ϕ (solid black line). This turning rate is influenced by all fibers in the neighborhood whose orientation (example denoted by θ and red dashed line) is close enough to ϕ. The reverse action, that is the rearrangement form orientation ϕ to ϕ' obviously exists and is expressed by a green arrow with the $T(x,\phi,\phi')$ label. The vertical dotted line corresponds to the reference direction $\phi = 0$.

Based on this assumptions, we consider the statistical density function $f = f(t,x,\phi)$ determining the collagen fiber bundles, i.e. the probability to find a collagen fiber bundle at the instant of time $t > 0$ at point $x \in \mathscr{D} \subset \mathbb{R}^d$, $d \in \{1,2,3\}$, with the orientation angle $\phi \in \left[-\frac{\pi}{2}, \frac{\pi}{2}\right[$. We propose the following model

$$\begin{aligned} &\frac{\partial f}{\partial t}\left(t,x,\phi\right) = Q\left(f\right) \qquad \text{with collision operator } Q\left(f\right) \text{ given by} \\ &Q\left(f\right) = \int_{-\frac{\pi}{2}}^{\frac{\pi}{2}} \left(f\left(t,x,\phi'\right) T\left(x,\phi',\phi\right) - f\left(t,x,\phi\right) T\left(x,\phi,\phi'\right)\right) \mathrm{d}\phi', \end{aligned} \tag{1}$$

where $T\left(x,\phi,\phi'\right)$ denotes the turning rate of the collagen fiber bundles at point $x \in \mathscr{D}$ from orientation $\phi \in \left[-\frac{\pi}{2}, \frac{\pi}{2}\right[$ to orientation $\phi' \in \left[-\frac{\pi}{2}, \frac{\pi}{2}\right[$. Previously, similar modelling ideas have been used in swarming models [22, 23, 6], kinetic models for chemotaxis [34, 35, 8], and kinetic models for tissue remodelling [10]. Following [22, 6] we define the turning rate as

$$T\left(x,\phi,\phi'\right) = \int_{\mathscr{D}} \int_{-\frac{\pi}{2}}^{\frac{\pi}{2}} \kappa\left(x-y\right) \omega\left(\phi-\phi',\phi-\theta\right) \mu^{\theta}\left(f\left(t,y,\bullet\right)\right) \mathrm{d}\theta \, \mathrm{d}y, \tag{2}$$

where $\kappa(x)$ and $\omega\left(\widetilde{\phi},\widetilde{\theta}\right)$ are the space kernel and the orientation kernel, respectively, describing the range of interactions between the fiber bundles. The kernels are weighted by $\mu^{\theta} : L^1\left(\left[-\frac{\pi}{2}, \frac{\pi}{2}\right[\right) \mapsto]0,1]$, that is a non-linear function of the density of the fiber bundles defined by

$$\mu^{\theta}(F) := \frac{F(\theta)}{\int_{-\frac{\pi}{2}}^{\frac{\pi}{2}} F(\theta') \, \mathrm{d}\theta'}.$$

The turning rate $T\left(x,\phi,\phi'\right)$ given by (2) averages, with the non-linear weight μ^{θ}, the influence of all fibres in the neighbourhood restricted by both kernels.

Concerning the kernels $\kappa(x)$ and $\omega\left(\widetilde{\phi},\widetilde{\theta}\right)$, first, we notice again that the interactions between the fibers are mediated by tenocytes. Relatively large cell size compared to fiber bundles leads us to the assumption about the typical long-range interactions with scope related to the cell size, which we model by the space kernel $\kappa(x)$. The orientation kernel $\omega\left(\widetilde{\phi},\widetilde{\theta}\right)$ (which is π-periodic with respect to both variables) describes the influence of the orientation of fiber bundles in the neighborhood. We assume that the change from orientation ϕ to orientation ϕ' arises from interactions with all neighboring fiber bundles whose orientations are denoted by θ. Therefore, the orientation kernel $\omega\left(\widetilde{\phi},\widetilde{\theta}\right)$ depends on $\widetilde{\phi} = \phi - \phi'$ which is the deviation between original orientation ϕ and orientation to become ϕ' and $\widetilde{\theta} = \phi - \theta$ which is the deviation between original orientation ϕ and any orientation θ that causes the change to the orientation ϕ'. The simplest example of space kernel is given by $\kappa_0(x) = \kappa_o \delta(x)$ where δ is the delta

Dirac function. Other typical examples of spatial and orientation kernels are given by finite distance interactions, that is

$$\kappa_R(x) = \begin{cases} \frac{\kappa_0}{B_R} & |x| \le R \\ 0 & |x| \ge R \end{cases} \qquad \text{and} \qquad \omega_\sigma\left(\widetilde{\phi},\widetilde{\theta}\right) = \bar{g}_\sigma\left(\widetilde{\phi}-\widetilde{\theta}\right). \tag{3}$$

with

$$\bar{g}_\sigma(s) = \begin{cases} \frac{1}{2\sigma} & |s| \le \sigma \\ 0 & |s| \ge \sigma \end{cases}. \tag{4}$$

Here, B_R refers to the area of euclidean ball of radius R in dimension d. Other kernels can be periodized exponential approximation of the Dirac Deltas as in [22, subsection 2.2].

3.1 Asymptotic Fokker-Planck Model Reduction

To derive a reduced Fokker-Planck-like collision operator, we follow the strategy described in [6] for swarming models reminiscent of similar approaches used in granular media descriptions [44, 5], social phenomena such opinion dynamics [45, 24], and wealth distribution models [11]. This approach comes back to grazing collision limits in kinetic theory [13, 43]. Let assume that except on a neighbourhood of $\widetilde{\phi} = 0$, the orientation kernel $\omega\left(\widetilde{\phi},\widetilde{\theta}\right)$ is negligible.

Hypothesis 1. *For small enough ε there exist two functions: a $\frac{\pi}{\varepsilon}$-periodic function $g \in L^\infty\left(\left[-\frac{\pi}{2\varepsilon},\frac{\pi}{2\varepsilon}\right[\right)$ and a π-periodic function $h:\mathbb{R}\mapsto\left[-\frac{\pi}{2},\frac{\pi}{2}\right[$ such that*

- *the orientation kernel satisfies the following scaling*

$$\omega_\varepsilon\left(\widetilde{\phi},\widetilde{\theta}\right) = g_\varepsilon\left(\widetilde{\phi}-\varepsilon h\left(\widetilde{\theta}\right)\right) \qquad \textit{with} \qquad g_\varepsilon(s) = \frac{1}{\varepsilon} g\left(\frac{s}{\varepsilon}\right).$$

- *for any $\widetilde{\phi} \in \left[-\frac{\pi}{2},-\varepsilon\frac{\pi}{2}\right] \cup \left[\varepsilon\frac{\pi}{2},\frac{\pi}{2}\right[$ we have $g_\varepsilon\left(\widetilde{\phi}\right) = O\left(\varepsilon^3\right)$.*

The periodicity assumptions on g and h provide that the orientation kernel $\omega\left(\widetilde{\phi},\widetilde{\theta}\right)$ is π-periodic with respect to both variables. We note that, g_ε equals to $\bar{g}_\varepsilon$ from (3) extended by zero to $\left[-\frac{\pi}{2\varepsilon},\frac{\pi}{2\varepsilon}\right[$ satisfies the assumption for ε small enough. Moreover, the construction of other C^∞ functions satisfying the properties based on approximations of this finite angle reorientation region is relatively straightforward. An example of a simple functions h satisfying our assumptions is $h(s) = \sin(2s)$.

Now, we focus on the turning rate T given by (2). We rewrite the model in the weak form, and for simplicity we express the nonlinear weight $\mu^\theta\left(f\left(t,y,\bullet\right)\right)$ as

$$\mu^\theta\left(f\left(t,y,\bullet\right)\right) = \frac{f\left(t,y,\theta\right)}{\rho\left(t,y\right)} \text{ with } \rho\left(t,y\right) := \int_{-\frac{\pi}{2}}^{\frac{\pi}{2}} f\left(t,y,\theta'\right)\mathrm{d}\theta'.$$

Multiplying the collision operator by a π-periodic test function of the orientation $\Psi \in L^2\left(\left[-\frac{\pi}{2},\frac{\pi}{2}\right[\right)$ and integrating over the orientation, we obtain

$$\begin{aligned}\int_{-\frac{\pi}{2}}^{\frac{\pi}{2}} Q(f)\Psi(\phi)\,\mathrm{d}\phi &= \int_{-\frac{\pi}{2}}^{\frac{\pi}{2}}\int_{-\frac{\pi}{2}}^{\frac{\pi}{2}} f(t,x,\phi)\,T(x,\phi,\phi')\left(\Psi(\phi')-\Psi(\phi)\right)\mathrm{d}\phi'\,\mathrm{d}\phi \\ &= \int_{\mathscr{D}}\int_{-\frac{\pi}{2}}^{\frac{\pi}{2}} \frac{f(t,y,\theta)}{\rho(t,y)}\kappa(x-y)\int_{-\frac{\pi}{2}}^{\frac{\pi}{2}} f(t,x,\phi)\,A(\phi,\theta)\,\mathrm{d}\phi\,\mathrm{d}\theta\,\mathrm{d}y\end{aligned}$$

with

$$A(\phi,\theta)=\int_{-\frac{\pi}{2}}^{\frac{\pi}{2}}\omega(\phi-\phi',\phi-\theta)\left(\Psi(\phi')-\Psi(\phi)\right)\mathrm{d}\phi'.$$

Then, using the Hypothesis 1 and Taylor expansion, we get

$$\begin{aligned}A(\phi,\theta) &= \int_{\phi-\varepsilon\frac{\pi}{2}}^{\phi+\varepsilon\frac{\pi}{2}}\omega(\phi-\phi',\phi-\theta)\left(\Psi(\phi')-\Psi(\phi)\right)\mathrm{d}\phi' + O(\varepsilon^3) \\ &= \int_{\phi-\varepsilon\frac{\pi}{2}}^{\phi+\varepsilon\frac{\pi}{2}}\omega(\phi-\phi',\phi-\theta)\left((\phi'-\phi)\Psi'(\phi)+\frac{(\phi'-\phi)^2}{2}\Psi''(\phi)\right)\mathrm{d}\phi' + O(\varepsilon^3) \\ &= G_1(\phi-\theta)\Psi'(\phi)+G_2(\phi-\theta)\Psi''(\phi)+O(\varepsilon^3),\end{aligned}$$

with the parameters

$$G_a(\widetilde{\theta})=\frac{\varepsilon^a}{a}\int_{-\frac{\pi}{2}}^{\frac{\pi}{2}}\beta^a g\left(\beta-h(\widetilde{\theta})\right)\mathrm{d}\beta, \qquad \text{where} \qquad a\in\{1,2\}.$$

Thus, the collision operator can be approximated as

$$\int_{-\frac{\pi}{2}}^{\frac{\pi}{2}} Q(f)\Psi(\phi)\,\mathrm{d}\phi \simeq \int_{-\frac{\pi}{2}}^{\frac{\pi}{2}}\left(-C(t,x,\phi)\,\partial_\phi\Psi + D(t,x,\phi)\,\partial_\phi^2\Psi\right) f(t,x,\phi)\,\mathrm{d}\phi + O(\varepsilon^3).$$

We can rewrite it in the classical formulation by integrating by parts to obtain a nonlinear nonlocal approximation of our integral operator by

$$Q(f)\simeq\frac{\partial}{\partial\phi}\left(C[f](t,x,\phi)\,f+\frac{\partial}{\partial\phi}\left(D[f](t,x,\phi)\,f\right)\right)+O(\varepsilon^3)$$

where

$$C[f](t,x,\phi)=\int_{-\frac{\pi}{2}}^{\frac{\pi}{2}} K[f](t,x,\theta)\,G_1(\phi-\theta)\,\mathrm{d}\theta, \tag{5}$$

$$D[f](t,x,\phi)=\int_{-\frac{\pi}{2}}^{\frac{\pi}{2}} K[f](t,x,\theta)\,G_2(\phi-\theta)\,\mathrm{d}\theta, \tag{6}$$

and

$$K[f](t,x,\theta) = \int_{\mathscr{D}} \frac{\kappa(x-y) f(t,y,\theta)}{\rho(t,y)} \, \mathrm{d}y.$$

Therefore, we can reduce the complexity of our model to the nonlinear nonlocal Fokker-Planck equation

$$\frac{\partial f}{\partial t}(t,x,\phi) = \frac{\partial}{\partial \phi}\left(C[f](t,x,\phi) f + \frac{\partial}{\partial \phi}\left(D[f](t,x,\phi) f \right) \right). \tag{7}$$

Notice that it is straightforward to check that a Dirac Delta centered at a given orientation is a stationary weak solution of (7) in the particular case of both g and κ to be Dirac Deltas at 0 as soon as $h(0) = 0$.

4 Computational simulation

The following section consists of two parts. First we provide necessary details on the numerical scheme developed to numerically approximate (7). Then we present the actual simulation results together with a discussion on the impact of particular parameters on observed dynamics. We conclude the subsection with considerations on the possible biological interpretation of the results.

4.1 Numerical scheme

To approximate the solution of the Fokker-Planck like model (7) we use a classical explicit Euler finite volume scheme with an upwind finite volume discretization. To this end, we rewrite the model (7) in the form of a nonlinear continuity equation

$$\frac{\partial}{\partial t} f(t,x,\phi) + \frac{\partial}{\partial \phi}\left(f(t,x,\phi) U[f](t,x,\phi) \right) = 0, \tag{8}$$

where

$$U[f](t,x,\phi) := -\left(C[f] + \frac{\partial}{\partial \phi} D[f] + D[f] \frac{\partial}{\partial \phi} \log f \right)(t,x,\phi). \tag{9}$$

Consider a regular grid of N_x points in space and N_ϕ points in orientation. Let $\delta_x = \frac{1}{N_x}$ and $\delta_\phi = \frac{\pi}{N_\phi}$ be the space step and the orientation step, whereas the discrete time $t^{n+1} = t^n + \delta_t^n$ with the time step δ_t^n defined by CFL condition (11). We denote by $n \in \mathbb{N}$ the time index, by $k \in [0, N_x - 1] \cap \mathbb{N}$ the space index and by $j \in [0, N_\phi - 1] \cap \mathbb{N}$

the orientation index. Now $f^n_{k,j}$ stands for an approximation of $f\left(t^n, k\delta_x, j\delta_\phi\right)$. The explicit Euler scheme with an upwind finite volume discretization of (8) reads as

$$\begin{aligned} f^{n+1}_{k,j} = f^n_{k,j} - \frac{\delta^n_t}{\delta_\phi}\Big(f^n_{k,j}\Big(\Big(U^n_{k,j+1/2}\Big)_+ + \Big(U^n_{k,j-1/2}\Big)_-\Big) \\ - f^n_{k,j+1}\Big(U^n_{k,j+1/2}\Big)_- - f^n_{k,j-1}\Big(U^n_{k,j-1/2}\Big)_+\Big) \end{aligned} \tag{10}$$

where the positive and negative part functions was used, i.e. $(\psi)_\pm = \frac{|\psi|\pm\psi}{2}$. We define the approximation of the velocity $U\left(n\delta^n_t, x_k, \phi\right)$ at the interface $\phi = \left(j+1/2\right)\delta_\phi$ by

$$U^n_{k,j+1/2} = -\left(C^n_{k,j+1/2} + \frac{D^n_{k,j+1} - D^n_{k,j}}{\delta_\phi} + D^n_{k,j+1/2}\frac{\log f^n_{k,j+1} - \log f^n_{k,j}}{\delta_\phi}\right).$$

For the convenience of the reader we remark that time step δ^n_t satisfy the CFL condition if there exists $0 < \lambda \leq 1$ such that for any $k \in [1, N_x] \cap \mathbb{N}$ and $j \in \left[1, N_\phi\right] \cap \mathbb{N}$, we have

$$\delta^n_t \leq \frac{\lambda\delta_\phi}{U^n_{k,j+1/2}}. \tag{11}$$

If the CFL condition is satisfied, then the upwind scheme preserves the positivity of the solution.

We propose the first-order numerical scheme for both orientation and time. We note that with the use of methods such as MUSCL or WENO for the discretization of the orientation derivative and a Runge-Kutta scheme for time discretization, it is possible to obtain higher accuracy. However, for our purposes, the proposed solution is sufficient. For more information on related finite volume discretizations, we refer the reader to papers [9, 4].

It remains us to define the coefficients $C^n_{k,j+1/2}$, and $D^n_{k,j+m/2}$ for $m \in \{0,1\}$. Let us remark that those coefficients are in fact convolution products in orientation and in space, respectively. The discrete integral of A_i, where $i \in [0, N-1] \cap \mathbb{N}$ is defined by

$$\langle A_\star \rangle = \frac{1}{N}\left(\frac{A_1 + A_2}{2} + \sum_{j=1}^{N-2} A_i\right)$$

Now, we introduce the discrete counterpart of the convolution product. The discrete convolution product of A_i and B_i, where $i \in [0, N-1] \cap \mathbb{N}$ is defined for any $j \in [0, N-1] \cap \mathbb{N}$ by

$$[A_\star * B_\star]_j = \langle A_\star B_{\underline{j-\star}_N} \rangle$$

where $\underline{n}_N = n - N\left\lfloor \frac{n}{N} \right\rfloor$ is the modulo operator and N stands for N_x or $N_\phi + 1$ (because of the periodic bound) depending on whether we consider the space or the orientation convolution product. The star $\star$ denotes the variable on which the convolution product acts in the case of several indexes.

The discrete counterparts of the operators $C[f]$ from (5) and $D[f]$ from (6) are defined as following

$$C^n_{k,j+1/2} = \pi \left[K^n_{k,\star} * G_{1,\star} \right]_{j+1/2} \qquad \text{and} \qquad D^n_{k,j+m/2} = \pi \left[K^n_{k,\star} * G_{2,\star} \right]_{j+m/2},$$

where $m \in \{0,1\}$,

$$K^n_{k,j} = |\mathscr{D}| \left[\frac{f^n_{\star,j}}{\rho^n_\star} * \kappa_\star \right]_k \qquad \text{with} \qquad \kappa_k = \kappa(x_k)$$

and coefficients $G_{a,j+m/2}$ are the approximations of the functions $G_a\left(\left(j+m/2\right)\delta_\phi\right)$.

For the $\omega\left(\widetilde{\theta},\widetilde{\phi}\right)$ simple enough, it is possible to obtain analytically the function $G_a\left(\widetilde{\theta}\right)$, however for the general case of $\omega\left(\widetilde{\theta},\widetilde{\phi}\right)$, one can use the approximation

$$G_{a,j+m/2} = \frac{\varepsilon^a \pi}{a} \langle \widetilde{G}^{a,j+m/2}_\star \rangle \qquad \text{and}$$

$$\widetilde{G}^{a,j+m/2}_i = \left(\left(i\delta_\phi - \frac{\pi}{2} \right) \right)^a g\left(\left(i\delta_\phi - \frac{\pi}{2} \right) - h\left(\left(j+m/2 \right)\delta_\phi \right) \right),$$

for $j \in \left[0, N_\phi\right] \cap \mathbb{N}$ and $i \in \left[0, N_\phi\right] \cap \mathbb{N}$. Note, that these parameters are computed only once at the initial state and do not depend on the solution state. The density of the distribution f naturally reads $\rho^n_k = \pi \langle f^n_{k,\star} \rangle$.

4.2 Computational simulation

In this subsection, we present the results of the numerical simulation of the reduced Fokker-Planck type model (7). To present them in a clear way, we consider a 1D space domain $\mathscr{D} = [0,1]$. We specify functions $\kappa(\widetilde{x}) = \kappa_R(\widetilde{x})$ as defined by (3), $g_\varepsilon(s) = \overline{g}_\sigma(s)$ as defined by (4), and finally we set $h\left(\widetilde{\theta}\right) = \sin\left(2\widetilde{\theta}\right)$. The coefficient κ_0 is fixed to 1, whereas the other two, $R > 0$ and $\sigma > 0$ varies in respective simulations, as we analyze their influence on the dynamics of the solution. As the initial condition, we take the function

$$f\left(0,x,\phi\right) = \frac{f^0\left(x,\phi\right)}{\int_{-\frac{\pi}{2}}^{\frac{\pi}{2}} f^0(x,\theta)\,\mathrm{d}\theta},$$

where

$$f^0\left(x,\phi\right) = \sum_{i=1}^{4} \exp\left(-\frac{\sigma^0_i}{x(1-x)} \left(\phi - \left(\frac{1}{2} + A^0_i \sin\left(\omega^0_i x\right) \right) \pi \right)^2 \right), \tag{12}$$

and parameters σ^0_i, A^0_i, and ω^0_i are given as

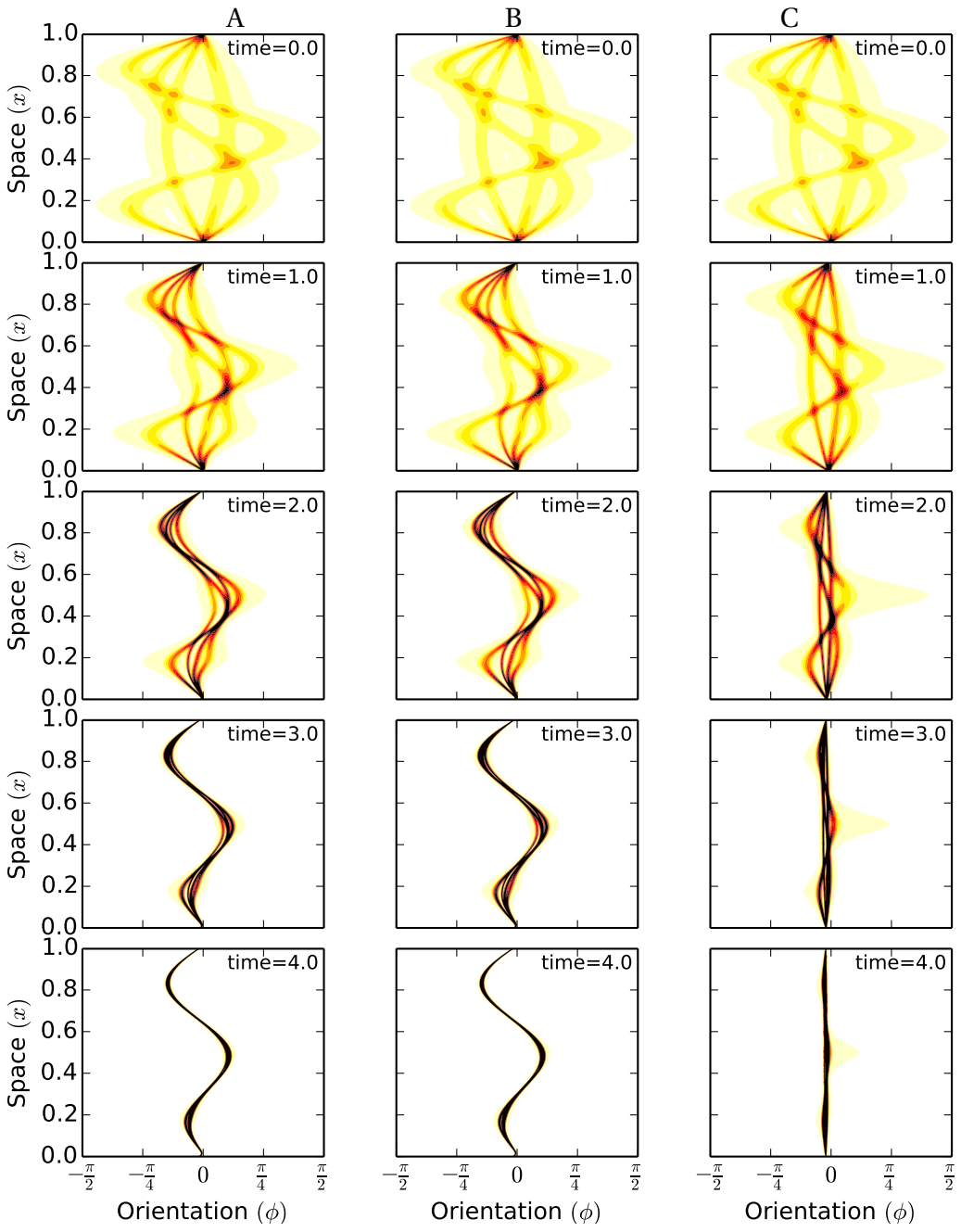

Figure 5: Time evolution of the solution to the model (7) performed for different sets of parameters R and σ, i.e.column A – $R = 10^{-2}$ and $\sigma = 10^{-3}\pi$; column B – $R = 10^{-2}$ and $\sigma = 10^{-1}\pi$; and column C – $R = 1$ and $\sigma = 10^{-3}\pi$. Color intensity represents the importance of density.

i	1	2	3	4
σ_i^0	10	10	5	20
A_i^0	0.1	0.2	-0.3	-0.15
ω_i^0	π	2π	3π	π

For all the simulation, the time step is computed using the CFL condition (11) with the parameter $\lambda = 1$.

In Figure 5 we show the time evolution of the solution to the numerical scheme presented in Section 4.1 obtained for three sets of parameters, with the orientation and space resolutions set to $N_\phi = 1000$ and $N_x = 500$, respectively. Columns A, B and C present results attained for $R = 10^{-2}$ and $\sigma = 10^{-3}\pi$, $R = 10^{-2}$ and $\sigma = 10^{-1}\pi$, $R = 1$ and $\sigma = 10^{-3}\pi$, respectively. The numerical simulations we performed suggest that parameter σ does not have a major impact on the results, whereas the parameter R influences the results a lot. To bolster this hypothesis, we have run a set of 150 simulations (with $N_\phi = N_x = 300$) with the same initial condition (12), and parameters R and σ ranging from 10^{-2} to 1, and then we analyzed the results.

In order to asses more precisely the impact of the investigated parameters we define τ to be the time needed for the variance of f to become smaller than 10% of the variance of the initial distribution (12). Time τ is defined such that for any n such that $t^n > \tau$, we have $V^n \leq 10^{-1} V^0$ where

$$V^n = \pi \left\langle \left(\theta_\star - \overline{\theta}^n\right)^2 F_\star^n \right\rangle \qquad \text{with} \qquad \theta_j = j\delta_\phi - \frac{\pi}{2},$$

$$\overline{\theta}^n = \pi \left\langle \theta_\star F_\star^n \right\rangle, \qquad \text{and} \qquad F_j^n = |\mathscr{D}| \left\langle f_{\star,j}^n \right\rangle.$$

Figure 6 presents a map of the relationship between time τ and values of parameters R and σ created based on 150 simulations carried out. We observe that as the parameter R decreases to 0 time, τ tends to infinity. Contrarily to R, the parameter σ does not influence the solution significantly, except for the case when it is about the size of the orientation domain, i.e. π.

Again referring to Figure 5 one can observe that for for any point in space x, the solution tends to a Dirac function in the orientation phase. However, for larger values of R (column C) the center of the Dirac function is reached for the same orientation ϕ, whereas for R small enough (columns A and B) the center of the Dirac function depends significantly on x.

From biological perspective, by choosing function (12) as the initial condition we intended to get, within the 1D framework, a simple representation of a tendon being after surgical reconstruction and at the end of the proliferative stage of healing, when the rearrangement of fibers begins. The purpose we aimed while performing numerical simulations was to identify the parameters that actually influence the dynamics of

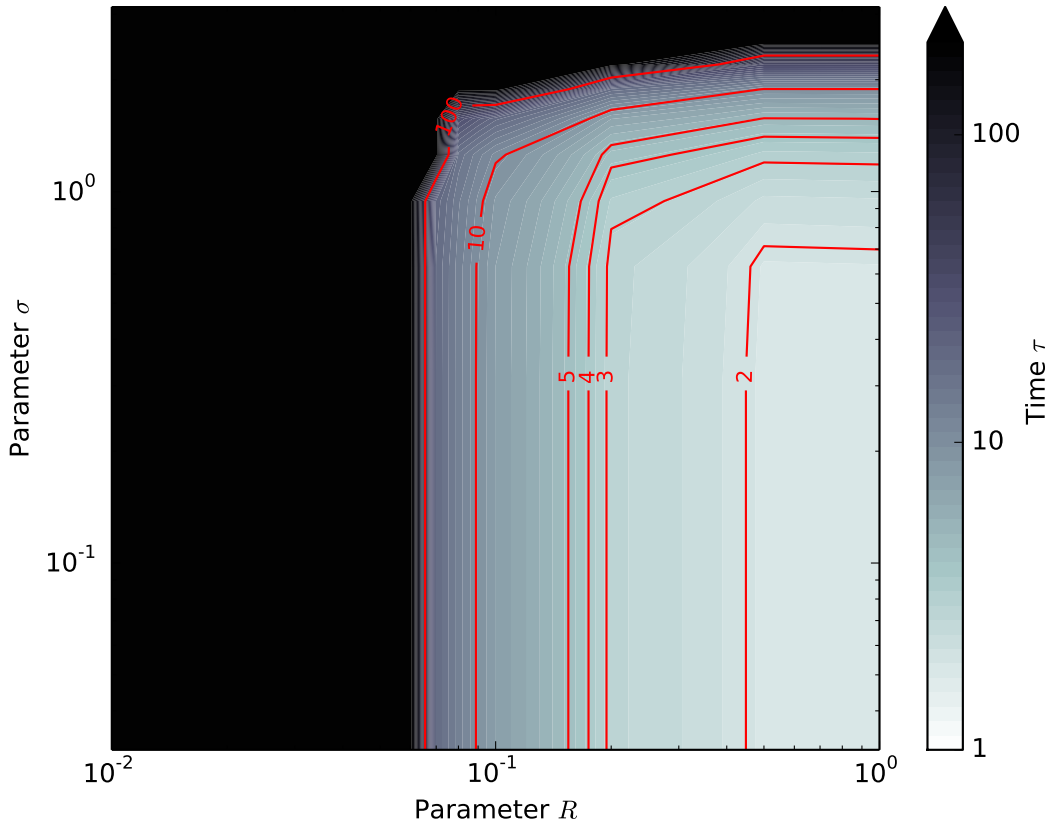

Figure 6: Characteristic time of the dynamic τ as function of the parameters R and σ (log scale).

the solution, and consequently to identify factors that might be important for the dynamics of tendon healing. The obtained results suggest that the range of spatial interactions influences the dynamics a lot whereas, the size of the orientation kernel does not have a major impact on the result, see Figure 5, results corresponding to small range interactions both in space and orientation; small range interaction in space and long-range interactions in orientation; and long-range interaction in space and small range interactions in orientation, are shown in columns A, B, and C, respectively. Assuming that the range of spatial interactions is related to the size of the tenocytes, and not forgetting other crucial factors such as the rate of collagen synthesis, we hypothesize that the size of tenocytes also plays a role in the course of tendon healing. This could explain, at least in part, the importance of physical exercises in returning patients' recovery. It is known from clinical practice that proper rehabilitation exercises are crucial for the healing process however, it is not entirely clear why. A possible ex-

planation is that the physical load affects the shape and size of the tenocytes. Without prejudging whether this working hypothesis is true, it is an important research topic for further investigation.

5 Conclusions

Tendon injuries give rise to significant morbidity, and at present only limited scientifically proven management modalities exist. A better understanding of tendon function and healing will allow specific treatment strategies to be developed. However, considering the complexity and multistage character of the tendon healing, a sensible strategy is to develop partial models of examined processes at first. Therefore, we restrict our attention to the latter stage of the healing process that consists mainly of the tenocytes mediated reconstruction of the parallel structure of collagen bundles. The size of tenocytes, which is noticeable compared to the size of the collagen bundles, prompts us to capture their effect in non-local terms. Therefore we propose an integro-differential equation to describe the dynamics of the statistical density of collagen bundles distribution, with non-local terms standing for fibers' mutual influence. The proposed model contains two non-local kernels to capture the range of spatial and orientational influences. These two kernels require estimation before running the predictive simulations. Unfortunately, the numerical cost of the computation needed makes the estimation of the parameters with data assimilation tools very difficult. Therefore, we propose a proper model reduction that is suitable for applications.

The result, that might be of biological relevance, is the following working hypothesis that needs further investigation: the importance of tenocyte size for the tendon healing process. Moreover, we would like to emphasize the importance of model reduction. Nowadays, the majority of mathematical models, although interesting and providing a qualitative explanation of some phenomena, usually are missing a genuine connection to experimental data. The missing connection is particularly acute for models describing disease processes and response to treatment. Largely it is due to the difficulty of establishing proper experimental scenarios – that is precisely the case of tendon healing. A solution may come with new advances in medical imaging. At present, these images do not have the resolution sufficient to obtain *in vivo* information on the arrangement of collagen fibers, however, the progress is very fast. One can expect that high-grade data will soon become available allowing the inverse problem approach. Still, the inverse problem methodology requires huge computing resources. Considering these requirements the pertinent strategy may be an appropriate reduction of models, so as to simplify and shorten the numerical simulations while maintaining the essential features of the model.

Acknowledgements

J.A. Carrillo was partially supported by the EPSRC grant number EP/P031587/1. J.A. Carrillo and M. Parisot acknowledge the support from Institute of Mathematics, Polish Academy of Sciences within the framework "Małe spotkania badawcze". Z. Szymańska was supported by the National Science Centre Poland Grant 2017/26/M/ST1/00783. All medical image data were obtained within the National Centre for Research and Development Grant STRATEGMED1/233224/10/NCBR/2014.

References

[1] J. Banasiak and M. Lachowicz. Kinetic model of alignment. In Methods of Small Parameter in Mathematical Biology. Modeling and Simulation in Science, Engineering and Technology, chapter 7, pages 195–221. Birkhäuser, Cham, 2014.

[2] M. Benjamin and J. Ralphs. Tendon and ligaments – an overview. Histol. Histopathol., 12(4):1135–1144, 1997.

[3] P.K. Beredjiklian. Biologic aspects of flexor tendon laceration and repair. J Bone Joint Surg Am, 85(3):539–550, 2003.

[4] J. A. Carrillo, Alina Chertock, and Yanghong Huang. A finite-volume method for nonlinear nonlocal equations with a gradient flow structure. Communications in Computational Physics, 17(01):233–258, 2015.

[5] J.A. Carrillo, S. Cordier, and G. Toscani. Over-populated tails for conservative-in-the-mean inelastic Maxwell models. Discrete Contin. Dyn. Syst. A., 24(1):59–81, 2009.

[6] J.A. Carrillo, R. Eftimie, and F. Hoffmann. Non-local kinetic and macroscopic models for self-organised animal aggregations. Kinet. Relat. Models, 8(3):413–441, 2015.

[7] J.A. Carrillo, M. Fornasier, J. Rosado, and G. Toscani. Asymptotic flocking dynamics for the kinetic Cucker-Smale model. SIAM J. Math. Anal., 42:218–236, 2010.

[8] J.A. Carrillo and B. Yan. An asymptotic preserving scheme for the diffusive limit of kinetic systems for chemotaxis. Multiscale Model. Simul., 11(1):336–361, 2013.

[9] C. Chainais-Hillairet and F. Filbet. Asymptotic behaviour of a finite-volume scheme for the transient drift-diffusion model. IMA J. Numer. Anal., 27(4):689–716, 2007.

[10] A. Chauviere, L. Preziosi, and T. Hillen. Modeling the motion of a cell population in the extracellular matrix. Discrete Contin. Dyn. Syst. A., Dynamical systems and differential equations. Proceedings of the 6th AIMS International Conference, suppl.:250–259, 2007.

[11] S. Cordier, L. Pareschi, and G. Toscani. On a kinetic model for a simple market economy. J. Stat. Phys., 120(1-2):253–277, 2005.

[12] L.E. Dahners. Growth and development of tendons. In N. Maffulli, P. Renström, and W.B. Leadbetter, editors, Tendon Injuries, chapter 3, pages 22–24. Springer-Verlag, London, 2005.

[13] P. Degond and B. Lucquin-Desreux. The Fokker-Planck asymptotics of the Boltzmann collision operator in the Coulomb case. Math. Models Methods Appl. Sci., 2(2):167–182, 1992.

[14] P. Degond and S. Motsch. Continuum limit of self-driven particles with orientation interaction. Math. Models Methods Appl. Sci., 18(suppl.):1193–1215, 2008.

[15] D. Docheva, S.A. Müller, M. Majewski, and H.E. Evans. Biologics for tendon repair. Adv. Drug Deliv. Rev., 84:222–239, 2015.

[16] M. Doumic, M. Hoffmann, N. Krell, and L. Robert. Statistical estimation of a growth-fragmentation model observed on a genealogical tree. BERNOULLI, 21(3):1760 – 1799, 2015.

[17] M. Doumic, P. Maia, and J.P. Zubelli. On the calibration of a size-structured population model from experimental data. Acta Biotheor., 58(4):405 – 413, 2010.

[18] M. Doumic, A. Marciniak-Czochra, B. Perthame, and J.P. Zubelli. A structured population model of cell differentiation. SIAM J Appl Math., 71(6):1918 – 1940, 2011.

[19] M. Doumic, B. Perthame, and J.P. Zubelli. Numerical solution of an inverse problem in size-structured population dynamics. Inverse Probl., 25(4):25pp, 2009.

[20] G. Dudziuk, M. Lachowicz, H. Leszczyński, and Z. Szymańska. A simple model of collagen remodeling. Discrete Contin. Dyn. Syst. Ser. B., 24(5):2205–2217, 2019.

[21] R. Eftimie, G. de Vries, and M.A. Lewis. Complex spatial group patterns result from different animal communication mechanisms. PNAS, 104(17):6974–6979, 2007.

[22] R.C. Fetecau. Collective behavior of biological aggregations in two dimensions: a nonlocal kinetic model. Math. Modelels Methods Appl. Sci., 21(07):1539, 2011.

[23] R.C. Fetecau and R. Eftimie. An investigation of a nonlocal hyperbolic model for self-organization of biological groups. J. Math. Biol., 61(4):545–579, 2009.

[24] G. Furioli, A. Pulvirenti, E. Terraneo, and G. Toscani. Fokker-Planck equations in the modeling of socio-economic phenomena. Math. Models Methods Appl. Sci., 27(1):115–158, 2017.

[25] G. Jull, A. Moore, D. Falla, J. Lewis, C. McCarthy, and M. Sterling. Grieve's Modern Musculoskeletal Physiotherapy. Elsevier, 2015.

[26] D. Kader, M. Mosconi, F. Benazzo, and N. Maffulli. Achilles tendon rupture. In N. Maffulli, P. Renström, and W.B. Leadbetter, editors, Tendon Injuries, chapter 20, pages 187–200. Springer-Verlag, London, 2005.

[27] M. Kjær. Role of extracellular matrix in adaptation of tendon and skeletal muscle to mechanical loading. Physiol. Rev., 84(2):649–698, 2004.

[28] M. Lachowicz, H. Leszczyński, and M. Parisot. Blow-up and global existence for a kinetic equation of swarm formation. Math. Models Methods Appl. Sci., 27(6):1153–1175, 2017.

[29] H.Y. Li and Y.H. Hua. Achilles tendinopathy: Current concepts about the basic science and clinical treatments. Biomed Res Int, 2016:6492597, 2016.

[30] T.W. Lin, L. Cardenas, and L.J. Soslowsky. Biomechanics of tendon injury and repair. J Biomech, 37(6):865 – 877, 2004.

[31] V. Martinek, J. Huard, and F.H. Fu. Gene therapy in tendon ailments. In N. Maffulli, P. Renström, and W.B. Leadbetter, editors, Tendon Injuries, chapter 30, pages 307–312. Springer-Verlag, London, 2005.

[32] G. Nourissat, X. Houard, J. Sellam, D. Duprez, and F. Berenbaum. Use of autologous growth factors in aging tendon and chronic tendinopathy. Front. Biosci., E5:911–921, 2013.

[33] M. O'Brian. Anatomy of tendon. In N. Maffulli, P. Renström, and W.B. Leadbetter, editors, Tendon Injuries, chapter 1, pages 3–13. Springer-Verlag, London, 2005.

[34] H. G. Othmer, S. R. Dunbar, and W. Alt. Models of dispersal in biological systems. J. Math. Biol., 26(3):263–298, 1988.

[35] H.G. Othmer and T. Hillen. The diffusion limit of transport equations. II. Chemotaxis equations. SIAM J. Appl. Math., 62(4):1222–1250, 2002.

[36] M. Parisot and M. Lachowicz. A kinetic model for the formation of swarms with nonlinear interactions. Kinet. Relat. Models, 9(1):131–164, 2016.

[37] B. Perthame and J.P. Zubelli. On the inverse problem for a size-structured population model. *Inverse* Probl., 23(3):1037 – 1052, 2007.

[38] P. Sharma and N. Maffulli. Biology of tendon injury: healing, modeling and remodeling. J Musculoskelet Neuronal Interact, 6(2):181–190, 2006.

[39] P. Sharma and N. Maffulli. Tendinopathy and tendon injury: the future. Disabil Rehabil., 30:1733–45, 2008.

[40] J.G. Snedeker and J. Foolen. Tendon injury and repair - a perspective on the basic mechanisms of tendon disease and future clinical therapy. Acta Biomater., 63:18–36, 2017.

[41] N. Takahashi, P. Tangkawattana, Y. Ootomo, T. Hirose, J. Minaguchi, H. Ueda, M. Yamada, and K. Takehana. Morphometric analysis of growing tenocytes in the superficial digital flexor tendon of piglets. J. Vet. Med. Sci., 79(12):1960–1967, 2017.

[42] C.T. Thorpe and H.R.C. Screen. Tendon structure and composition. In P. Ackermann and Hart D., editors, Metabolic Influences on Risk for Tendon Disorders. Advances in Experimental Medicine and Biology, chapter 1, pages 3–10. Springer, Cham, 2016.

[43] G. Toscani. The grazing collisions asymptotics of the non-cut-off Kac equation. RAIRO Modél. Math. Anal. Numér., 32(6):763–772, 1998.

[44] G. Toscani. One-dimensional kinetic models of granular flows. M2AN Math. Model. Numer. Anal., 34(6):1277–1291, 2000.

[45] G. Toscani. Kinetic models of opinion formation. Commun. Math. Sci., 4(3):481–496, 2006.

[46] F. Wu, M. Nerlich, and D. Docheva. Tendon injuries: Basic science and new repair proposals. EFORT Open Rev., 2:332–342, 2017.

[47] G. Yang, B.B. Rothrauff, and R.S. Tuan. Tendon and ligament regeneration and repair: Clinical relevance and developmental paradigm. Birth Defects Res C, Embryo Today, 99(3):203–222, 2013.

[48] K.A. Young, J.A. Wise, P. DeSaix, D.H. Kruse, B. Poe, E. Johnson, J.E. Johnson, O. Korol, J. Gordon Betts, and M. Womble. Anatomy & Physiology. OpenStax, 2013.